



1

2 **The Aerosol Module in the Community Radiative Transfer Model** 3 **(v2.2 and v2.3): accounting for aerosol transmittance effects on the** 4 **radiance observation operator**

5 Cheng-Hsuan (Sarah) Lu^{1,2}, Quanhua Liu³, Shih-Wei Wei^{1,2}, Benjamin T. Johnson⁴, Cheng Dang¹,
6 Patrick G. Stegmann⁴, Dustin Grogan², Guoqing Ge^{5,6}, and Ming Hu⁶

7

8 ¹Joint Center for Satellite Data Assimilation, Boulder, CO, USA

9 ²Atmospheric Sciences Research Center, University at Albany, Albany, NY, USA

10 ³Center for Satellite Applications and Research, NOAA/NESDIS, College Park, MD, USA

11 ⁴Joint Center for Satellite Data Assimilation, College Park, MD, USA

12 ⁵Cooperative Institute for Research in Environmental Sciences, CU Boulder, CO, USA

13 ⁶Global System Laboratory, NOAA, Boulder, CO, USA

14

15 *Correspondence to:* Cheng-Hsuan Lu (clu@ucar.edu; clu4@albany.edu)

16 **Abstract**

17 The Community Radiative Transfer Model (CRTM), a sensor-based radiative transfer model, has been used within the
18 Gridpoint Statistical Interpolation (GSI) system for directly assimilating radiances from infrared and microwave sensors. We
19 conducted numerical experiments to illustrate how including aerosol radiative effects in CRTM calculations changes the GSI
20 analysis. Compared to the default aerosol-blind calculations, the aerosol influences reduced simulated brightness temperature
21 (BT) in thermal window channels, particularly over dust-dominant regions. A case study is presented, which illustrates how
22 failing to correct for aerosol transmittance effects leads to errors in meteorological analyses that assimilate radiances from
23 satellite IR sensors. In particular, the case study shows that assimilating aerosol-affected BTs affects analyzed temperatures in
24 the lower atmosphere significantly in several different regions of the globe. Consequently, a fully-cycled aerosol-aware
25 experiment improves 1-5 day forecasts of wind, temperature, and geopotential height in the tropical troposphere and Northern
26 Hemisphere stratosphere. Whilst both GSI and CRTM are well documented with online user guides, tutorials and code
27 repositories, this article is intended to provide a joined-up documentation for aerosol absorption and scattering calculations in
28 the CRTM and GSI. It also provides guidance for prospective users of the CRTM aerosol option and GSI aerosol-aware
29 radiance assimilation. Scientific aspects of aerosol-affected BT in atmospheric data assimilation are briefly discussed.



30 **1 Introduction**

31 An accurate and computationally efficient radiative transfer model is essential in radiance assimilation for supporting weather
32 prediction, physical retrievals for satellite environmental data records, and inter-comparison among remote sensing sensors.
33 The Community Radiative Transfer Model (CRTM) is a sensor-based radiative transfer model (Weng, 2007; Han et al., 2007).
34 It was primarily designed for computing satellite radiances and has been used within the Gridpoint Statistical Interpolation
35 (GSI, Wu et al., 2002; Kleist et al., 2009) system for directly assimilating radiances from infrared (IR) and microwave (MW)
36 sensors. Specifically, clear-sky radiance calculations are carried out within the CRTM given the atmospheric scattering and
37 absorption profile, surface emissivity and reflectivity, and source functions. For cloudy radiance simulations (Stegmann et al.,
38 2018), vertical profiles of hydrometeor variables (e.g., cloud liquid water path and ice water path) are also required. Note that
39 CRTM is not designed to describe longwave and shortwave broadband radiative transfer for general circulation model
40 applications. Instead, it is developed to support satellite radiance data assimilation and satellite retrieval development.

41
42 Past studies have demonstrated that aerosols significantly impact the simulation of brightness temperature (BT) in the IR
43 channels. BT is “a descriptive measure of radiation in terms of the temperature of a hypothetical blackbody emitting an
44 identical amount of radiation at the same wavelength” (American Meteorological Society, 2012). A reduction in retrieved BT
45 of 2°-4° K in the atmospheric window region due to a strong dust outbreak was reported during the Saharan Dust Experiment
46 (SHADE) campaign (Highwood et al., 2003). Pierangelo et al. (2004) and Peyridieu et al. (2009) showed that the dust cooling
47 effects may reach 3° K in tropical atmospheric conditions depending on the dust burden. Diaz et al. (2001) found that there is
48 a significant increase in the errors of sea surface temperature (SST) retrievals in the presence of enhanced aerosol loading in
49 the atmosphere. The dust effects on satellite derived SST are constrained by accounting for dust absorption (Weaver et al.,
50 2003), applying a dust correction scheme (Nalli and Stowe, 2002; Merchant et al., 2006), or removing dust-contaminated
51 observations (Divakarla et al., 2012).

52
53 Kim et al. (2018) used the Goddard Earth Observing System (GEOS)-atmospheric data assimilation system (ADAS) to
54 investigate the impact of aerosols on atmospheric data assimilation and radiative transfer. Wei et al. (2021) adopted the
55 methodology developed by Kim et al. (2018) and used the Global Data Assimilation System (GDAS) to assess the impact of
56 aerosol-affected BTs on the GDAS analysis. Note that GEOS-ADAS and GDAS both used GSI and CRTM, although the
57 version and configuration have differed. Both studies reported that: (i) a considerable cooling effect on simulated BT when
58 aerosols are considered; (ii) including aerosol transmittance effects in the BT calculation improves the fit to observations over
59 the dust-laden regions, and (iii) assimilating aerosol-affected radiance observations leads to a warmer atmospheric analysis in
60 lower levels.

61



62 Experiments conducted in Kim et al. (2018) and Wei et al. (2021) were based on the application of the CRTM aerosol
63 absorption and scattering routines. While aerosol absorption and scattering options are available from CRTM version 2.2
64 onwards; to our knowledge, the documentation of the CRTM aerosol module (Liu and Lu, 2016) has yet to be updated. Here
65 we presented a joined-up documentation for aerosol absorption and scattering calculations in the CRTM and GSI. In addition,
66 we provide guidance for prospective users of running aerosol-affected GSI analysis. Scientific aspects of aerosol-affected BT
67 in atmospheric data assimilation are also briefly discussed.

68 **2 GSI and CRTM**

69 Below, we provide a brief introduction to the GSI in section 2.1 and a description of the CRTM aerosol option in section 2.2.
70 In section 2.3, a description of running aerosol-aware GSI analysis is given here.

71 **2.1 GSI**

72 The multi-partner-developed GSI is an incremental three-dimensional variational (3D-Var) data assimilation system (Wu et
73 al., 2002; Kleist et al. 2009). GSI, alone or combined with an ensemble system, has been used widely by the modelling centers
74 and the research community for a range of research and applications. For instance, it is used operationally by the National
75 Oceanic and Atmospheric Administration (NOAA)/National Centers for Environmental Prediction (NCEP) for medium-range
76 weather forecast. It is also used by the National Aeronautics and Space Administration (NASA)/Global Modeling and
77 Assimilation Office (GMAO) for recent production of the Modern-Era Retrospective Analysis for Research and Applications,
78 version 2 (MERRA-2; Gelaro et al., 2017). The community version of the GSI system is supported and maintained by the
79 Developmental Testbed Center (DTC; <http://www.dtcenter.org>).

80
81 GSI can assimilate a wide range of observations, including conventional observations (such as radiosonde observations), radar
82 data, satellite retrievals (for example global positioning system (GPS) radio occultation sounding data), satellite radiance data,
83 etc. For IR satellite instruments, GSI has the capability to assimilate radiances from Advanced Infrared Sounder (AIRS) on
84 AQUA, Infrared Atmospheric Sounding Interferometer (IASI) on METOP-A and METOP-B, Cross-track Infrared Sounder
85 (CrIS) on S-NPP, High resolution Infrared Radiation Sounder (HIRS) on METOP-A, METOP-B, and NOAA-19, Advanced
86 Very High Resolution Radiometer (AVHRR) on NOAA-18 and METOP-A, Spinning Enhanced Visible and Infrared Imager
87 (SEVIRI) on M08 and M10, and Geostationary Operational Environmental Satellite (GOES) Sounders (s ndrD1, s ndrD2,
88 s ndrD3, and s ndrD4) on GOES-15. A comprehensive list of all observations assimilated and monitored by GDAS can be found
89 at the webpage for “Observational Data Processing at NCEP” ([https://www.emc.ncep.noaa.gov/emc/pages/infrastructure/obs-
90 data-processing.php](https://www.emc.ncep.noaa.gov/emc/pages/infrastructure/obs-data-processing.php)).

91



92 Despite the broad applications of GSI, the publicly released version of GSI handles only clear-sky radiances for IR
93 sensors. Without correcting for aerosol transmittance effects, systematic biases may be introduced into the meteorological re-
94 analysis fields when observations affected by aerosols are assimilated. The aerosol-aware option (discussed in section 2.2)
95 reduces such errors by enabling aerosols to influence GSI's radiance observation operator, CRTM, which calculates the BT
96 and Jacobians (radiance 1st derivative). This option, however, may degrade the data usage in GSI because the quality control
97 (QC) algorithm screens out observations based on measured BTs and aerosol-free simulated BTs. Thus, an improved QC
98 algorithm is needed to fully exploit radiance measurements under all sky conditions. The technical issues regarding the QC
99 procedure have been discussed in Kim et al. (2018) and Wei et al. (2021).

100 **2.2 CRTM aerosol module**

101 The CRTM, a one-dimensional radiative transfer model (Liu and Weng, 2006), is developed at the U.S. Joint Center for
102 Satellite Data Assimilation (JCSDA) with algorithm and software input from JCSDA funded research institutions. The CRTM
103 is composed of four modules, which include gaseous transmittance, surface emission and reflection, cloud and aerosol
104 absorption and scattering, and a solver for radiative transfer (Han et al., 2006). Given an atmospheric profile of temperature,
105 cloud and surface properties, and gaseous constituents and aerosol concentrations, the CRTM is called within the GSI to
106 calculate BTs for satellite sensors from IR sounders to MW imagers. Here, we describe the aerosol scattering and absorption
107 scheme in CRTM version 2. We refer the readers to Han et al. (2006) for the full details regarding CRTM version 1.
108

109 The CRTM version 2 has the optical look-up table for the Goddard Chemistry Aerosol Radiation and Transport (GOCART,
110 Chin et al., 2002; Colarco et al, 2010) model for the spectrum from ultraviolet to IR. The effect of aerosols on MW sensors is
111 not considered yet because the impact of aerosols on MW radiance is usually very small, given aerosols size is generally much
112 smaller than MW wavelengths (Petty, 2006). The optical tables from other aerosol models are not finalized yet, thus we discuss
113 mainly the GOCART model in this article.
114

115 The GOCART model (Chin et al., 2002; 2014), a bulk aerosol scheme, simulates major tropospheric aerosol components,
116 including dust, sea salt, black carbon (BC), organic carbon (OC) and sulfate. It is one of the most widely used aerosol modules
117 in the Weather Research and Forecasting model coupled with Chemistry (WRF-Chem; see Ukhov et al. (2021) and references
118 therein). It is used in the GEOS framework at GMAO for near-real-time aerosol forecasts (Colarco et al., 2010) as well as in
119 MERRA reanalysis (Bucharad et al., 2015) and MERRA-2 reanalysis (Randles et al., 2017). It is also implemented in the Global
120 Forecast System (GFS) framework at NCEP (Lu et al., 2016; Wang et al., 2018; Zhang et al., 2021) for near-real-time global
121 aerosol forecasts.
122

123 When GOCART was selected as the aerosol module within WRF-Chem, it was configured with fourteen GOCART aerosol
124 species (Liu et al., 2011): sulfate; hydrophobic and hydrophilic OC and BC; sea salt in four particle size bins (with radii of



125 0.1-0.5, 0.5-1.5, 1.5-5, and 5-10 μm) and dust particles in five particle size bins (with radii of 0.1-1.0, 1.0-1.8, 1.8-3, 3-6, and
126 6-10 μm). A default CRTM lookup-table has been used for pre-calculated aerosol optical property parameters such as mass
127 extinction, single scattering albedo, and asymmetry factor for the fourteen GOCART aerosol species (Liu et al., 2007; Liu and
128 Lu, 2016). We assume that the particles are spherical and externally mixed. We also assume lognormal size distributions for
129 sulfate and carbonaceous aerosols as well as for each sea salt and dust bin. The lognormal size distribution for N particles can
130 be expressed as follows (d'Almeida et al., 1991),

$$131 \quad n(\ln r) = \frac{N}{\sqrt{2\pi} \ln(\sigma_g)} \exp\left[-\frac{1}{2} \left(\frac{\ln r - \ln r_g}{\ln(\sigma_g)}\right)^2\right], \quad (1)$$

132 where r is a radius, r_g the geometric median radius, and σ_g the geometric mean standard deviation. The k^{th} moment of the
133 distribution can be expressed as follows (Binkowski and Roselle, 2003),

$$134 \quad M_k = \int_{-\infty}^{\infty} r^k n(\ln r) d\ln(r) = r_g^k \exp\left[\frac{k^2}{2} \ln^2(\sigma_g)\right]. \quad (2)$$

135 where M_0 is the number N of aerosol particles, and M_2 and M_3 are proportional to the total particulate surface area and volume,
136 respectively. Thus, the effective radius (r_{eff}) can be defined as

$$137 \quad r_{\text{eff}} = \frac{M_3}{M_2} = r_g \exp\left[\frac{5}{2} \ln^2(\sigma_g)\right]. \quad (3)$$

138
139 Table 1 lists the GOCART size parameters (particle density, effective radius, and geometric standard deviation) and refractive
140 indices at 550 nm used in CRTM version 2. The optical properties of each aerosol species is computed based on Mie scattering
141 theory. Hydrophilic aerosol particle size increases as relative humidity (RH) of the ambient atmosphere increases. Therefore,
142 the water content in aerosol needs to be considered when calculating the refractive index. The effective radius growth factor
143 for hygroscopic aerosols may be theoretically calculated or obtained from a pre-calculated look-up table (d'Almeida et al.,
144 1991). In this study, the hygroscopic growth factor used for the GOCART model (Chin et al., 2002) is adopted and given in
145 Table 2. Once the growth factor a_g is evaluated, the refractive index n_r for the hygroscopic aerosol can be calculated using a
146 volume mixing method as:

$$147 \quad n_r = n_w + (n_o - n_w) \times a_g^3 \quad (4)$$

148 where n_o and n_w are the refractive indices for dry aerosols and water, respectively. We adopt the refractive index n_o from
149 Optical Properties of Aerosols and Clouds (OPAC) dataset (Hess et al. 1998), while the water refractive index is given by
150 (Hale and Querry, 1973).

151
152 **Table 1.** Goddard Chemistry Aerosol Radiation and Transport (GOCART) size distribution parameters and refractive indices
153 at 550 nm for dry aerosols.



Aerosol type	Density [g cm ⁻³]	Effective radius r_{eff} [μm]	Standard deviation σ [μm]	Refractive index real part $n(\lambda)$	Refractive index imaginary part $k(\lambda)$
Sulfate	1.7	0.242	2.03	1.43	1.00×10^{-8}
OC1 (hydrophobic)	1.8	0.087	2.20	1.53	6.00×10^{-3}
OC2 (hydrophilic)	1.8	0.087	2.20	1.53	6.00×10^{-3}
BC1 (hydrophobic)	1.0	0.036	2.0	1.75	4.40×10^{-1}
BC2 (hydrophilic)	1.0	0.036	2.0	1.75	4.40×10^{-1}
SeaSalt1 (size range)	2.2	0.3	2.03	1.50	1.00×10^{-8}
SeaSalt2	2.2	1.0	2.03	1.50	1.00×10^{-8}
SeaSalt3	2.2	3.25	2.03	1.50	1.00×10^{-8}
SeaSalt4	2.2	7.5	2.03	1.50	1.00×10^{-8}
Dust1 (size range)	2.6	0.65	2.0	1.53	5.50×10^{-3}
Dust2	2.6	1.4	2.0	1.53	5.50×10^{-3}
Dust3	2.6	2.4	2.0	1.53	5.50×10^{-3}
Dust4	2.6	4.5	2.0	1.53	5.50×10^{-3}
Dust5	2.6	8.0	2.0	1.53	5.50×10^{-3}

154

155 **Table 2.** Hygroscopic aerosol growth factor a_g as a function of the ambient relative humidity (RH).

RH(%)	0	50	70	80	90	95	99
Sulfate	1.0	1.4	1.5	1.6	1.8	1.9	2.2
Organic Carbon	1.0	1.2	1.4	1.5	1.6	1.8	2.2
Black Carbon	1.0	1.0	1.0	1.2	1.4	1.5	1.9
Sea Salt	1.0	1.6	1.8	2.0	2.4	2.9	4.8

156

157 The GOCART model used by GMAO and NCEP for aerosol forecast and reanalysis has evolved to use 5 sea salt size bins
 158 (with radii of 0.03-0.1, 0.1-0.5, 0.5-1.5, 1.5-5, and 5-10 μm). The first sub-micron sea salt bin was added to facilitate optical
 159 properties and aerosol-cloud interaction studies (Colarco et al., 2010), but was excluded from the previous GOCART versions
 160 as well as the WRF-Chem GOCART model. While GMAO's GEOS and NCEP's GFS contain fifteen GOCART aerosol
 161 species, the CRTM aerosol module has also not yet been modified to include the new added sub-micron sea salt bin (see Table
 162 1). To overcome this discrepancy, the latest GSI/CRTM release (i.e., GSI 3.7 and CRTM 2.3) combines the mixing ratios from
 163 the two sub-micron sea salt bins in order to use the aerosol optical property parameters from the original GOCART model.
 164 This limitation is acknowledged in this article and will be addressed in a future CRTM release (see section 4).

165

166 While the CRTM is primarily designed for computing satellite radiances, an additional module was added to CRTM by Liu
 167 and Lu (2016) to compute aerosol optical depth (AOD). This CRTM-AOD module enables the GSI system to assimilate AOD
 168 observations (Liu et al., 2011; Schwartz et al., 2012; Pagowski et al., 2014). This article, however, is focused on the observation



169 operator for radiance, and we refer the reader to Pagowski et al. (2014) for the description of the AOD observation operator
170 and GSI AOD data assimilation.

171 **2.3 Running aerosol-aware GSI analysis**

172 The operational version GSI maintained by NOAA/NCEP Environmental Modeling Center (EMC) is utilized in the present
173 study. Its source code and associated static files are distributed through the GitHub repository ([https://github.com/NOAA-](https://github.com/NOAA-EMC/GSI)
174 [EMC/GSI](https://github.com/NOAA-EMC/GSI)). To run the GSI analysis, the reader can refer to the user guide for GSI v3.7 (the latest released version as of April
175 2021), which is available at https://dtcenter.ucar.edu/com-GSI/users/docs/users_guide/html_v3.7/index.html. In addition, an
176 online tutorial is available at https://dtcenter.ucar.edu/com-GSI/users/tutorial/online_tutorial/index_v3.7.php. For CRTM, the
177 user guide and tutorials can be found at <https://www.jcsda.org/jcsda-project-community-radiative-transfer-model>. Thus, only
178 a brief description of aerosol-affected BT calculations is given here.

179
180 A regression test “global_C96_fv3aerorad” has been introduced into NOAA/EMC GSI code repository (pull request #32) to
181 assure the functionality of aerosol-aware BT derivations in GSI/CRTM works as expected. This regression test uses a sample
182 background file taken from the aerosol member of the Global Ensemble Forecast System (GEFS-Aerosol; Zhang et al., 2021).
183 All fifteen GOCART aerosol species are passed along to the CRTM. In addition to the background file, a user needs to modify
184 the configuration files, anavinfo and satinfo, in the “fix” directory. The anavinfo file is the information file to set control and
185 analysis variables. The satinfo file is the information file to specify satellite channels to be assimilated and associated
186 parameters. For an aerosol-aware experiment where aerosol absorption and scattering are included in BT calculations, aerosol
187 species are specified in the “chem_guess” section of anavinfo and sensors and channels are set to 1 in the “iaerosol” column
188 of satinfo. The reader can refer to the fv3aerorad_satinfo.txt and anavinfo_fv3aerorad for the aerosol-aware configuration. The
189 corresponding namelist (gsiparm.anl) can be found at the “global_C96_fv3aerorad” section (line 2931–3046) in
190 regression_namelist.sh under the “regression” directory. It should be noted that the namelist variable, “lread_ext_aerosol”,
191 determines how GSI ingests the aerosol information from background files or external files

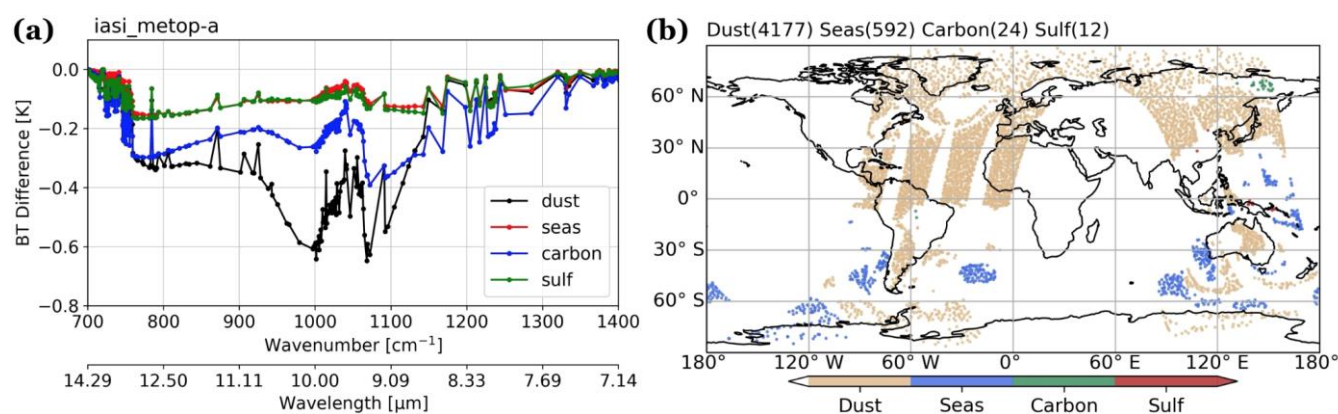
192 **3. Numerical Results**

193 **3.1 Aerosol impacts on BT calculations**

194 To illustrate how an aerosol transmittance correction is required within satellite radiances assimilated into meteorological data
195 assimilation systems, we present a detailed analysis of a single-cycle GSI experiment using GOCART fields from MERRA-2
196 on 12Z June 22, 2020. This time is chosen because it captures a strong Saharan dust loading event that covers the trans-Atlantic
197 region. A baseline GSI experiment with the anavinfo resource file reverted back to the default aerosol-blind configuration was
198 also conducted. Figure 1a shows the first-guess BT differences of IASI onboard METOP-A between the two experiments over
199 aerosol dominant regions (where the fraction of column mass density of dominant species is larger than 0.65, shown in Fig.



200 1b). Figure 1a shows that dust aerosols generate the strongest cooling effects, about 0.7° K at the thermal IR window region
 201 (~10 μm), than other species. The importance of correcting for aerosol transmittance effects within BT algorithms has been
 202 reported in previous studies (Sokolik, 2002; Weaver et al., 2003; Pierangelo et al., 2004; Matricardi, 2005; Merchant et al.,
 203 2006; Kim et al., 2018; Wei et al., 2021). Table 3 describes the range and the average of total aerosol column mass density
 204 over the regions with different dominant aerosol species. It shows that the total loading of aerosols is similar over the dust and
 205 carbonaceous aerosols dominated regions. This indicates that the stronger cooling effects by dust aerosol on BT in the IR
 206 window region is not due to stronger loading.
 207



208 **Figure 1.** (a) The differences (AER minus CTL) of first-guess brightness temperatures in the IR window region of IASI
 209 onboard METOP-A. (b) The corresponding regions dominated by different aerosol species from the 12Z June 22, 2020. The
 210 data counts for each species are labelled in panel (b).
 211
 212

213 **Table 3.** The range of aerosol column mass density (kg/m²) from MERRA-2 at the regions dominated by different aerosol
 214 species (fraction over 0.65) of IASI onboard METOP-A at the cycle of 12Z June 22, 2020.

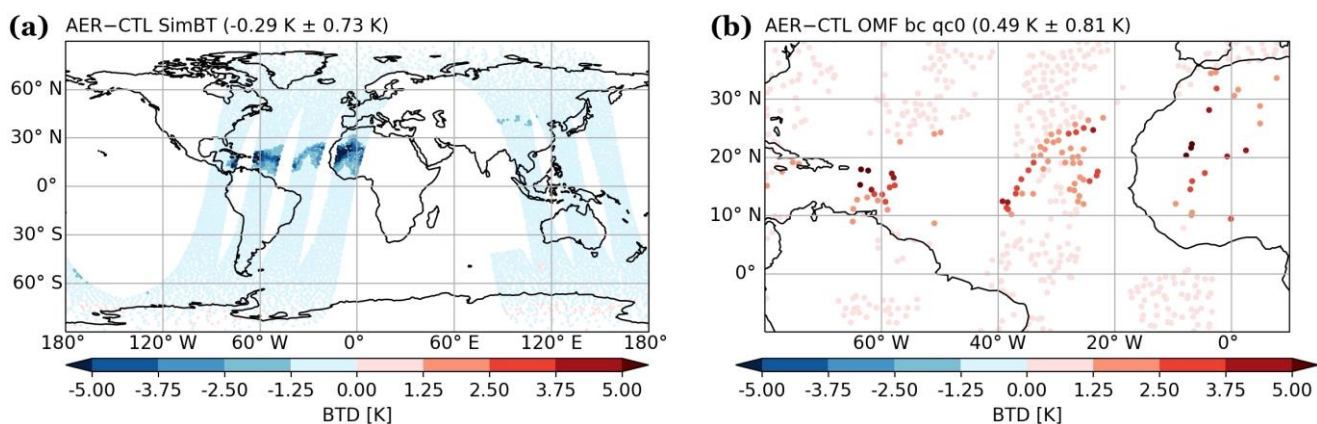
Dominant aerosol species	Column mass density (kg/m ²)		
	Minimum	Maximum	Average
Dust	2.69e-06	2.88e-03	1.76e-04
Sea salt	4.91e-06	4.01e-05	1.68e-05
BC+OC	1.04e-05	6.07e-04	1.76e-04
Sulfate	6.45e-06	9.53e-05	2.15e-05

215



216 Figure 2 displays the difference in the simulated BTs and first-guess departures at the 10.39 μm channel of IASI onboard
217 METOP-A between the two experiments. Significant aerosol cooling ($\sim 4^\circ\text{K}$) in BT was found over dust-laden areas in the
218 aerosol-aware experiment (Fig. 2a), including over North Africa and the trans-Atlantic region. Over the trans-Atlantic region,
219 the aerosol-aware experiment assimilated several observations with larger first-guess departures (Fig. 2b). When considering
220 aerosol information, the root-mean-square first-guess departures decreased 0.08°K globally and 0.25°K over the trans-
221 Atlantic region at this channel. This implies that simulated BTs in the aerosol aware run are in better agreement with the
222 observations.

223



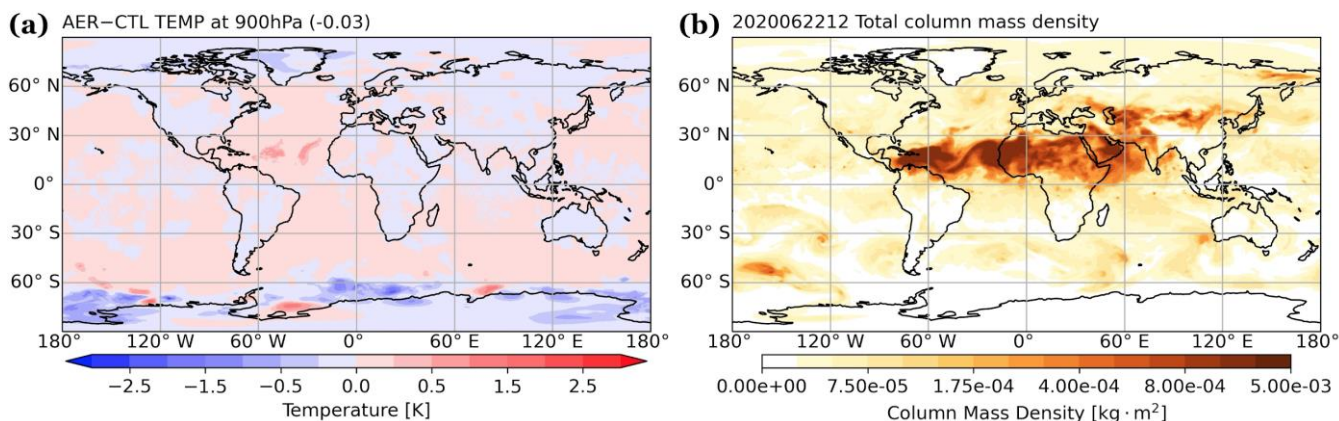
225

225 **Figure 2.** (a) Simulated BT and (b) first-guess departures differences (AER minus CTL) for 10.39 μm channel of IASI onboard
226 METOP-A. All the data are from the analysis cycle on 12Z June 22, 2020.

227

228 Figure 3 shows (a) the differences in analyzed temperature at 900 hPa between the two experiments and (b) the aerosol column
229 mass density incorporated in the GSI/CRTM system. When aerosol effects are considered in the BT calculations, the air
230 temperatures are not only adjusted over aerosol-laden regions but across the globe. The impact over aerosol-free regions could
231 be attributed to the change from the spatial correlation in the GSI background error covariance. For the trans-Atlantic region,
232 where the dust loading is high, the aerosol-aware experiment produces 0.5° to 1° of warming.

233



234

235

236

Figure 3. (a) The differences (AER minus CTL) of analyzed temperature (K) at 900 hPa and (b) the corresponding aerosol column mass density (kg m^{-2}) from MERRA-2 on 12Z June 22, 2020.

237

3.2 Aerosol impacts on the analysis

238

239

240

241

242

243

244

245

246

The experiments reported in this section were produced with the NCEP GFS version 14 and the corresponding GDAS. Our experiments used a coarser resolution, T670 (~30km) for the model and T254 (~80km) for the analysis, different from the NCEP operational GFSv14 configuration at T1534 (~13km) and T574 (~27km). The experiments covered the August 2017 period, initialized from NCEP's archived GDAS analysis on July 25 00Z. The control experiment (CTL_cyc) was an aerosol-blind fully cycled experiment where aerosol effects on radiances are not considered (as is by default). The aerosol experiment (AER_cyc) was an aerosol-aware fully cycled experiment where aerosol-affected satellite radiances are taken into account. Here, we used CRTM version 2.2.4. Time-varying 3-dimensional GOCART aerosols were taken from NCEP's archived NEMS GFS Aerosol Component (NGAC) v2 (Wang et al., 2018).

247

248

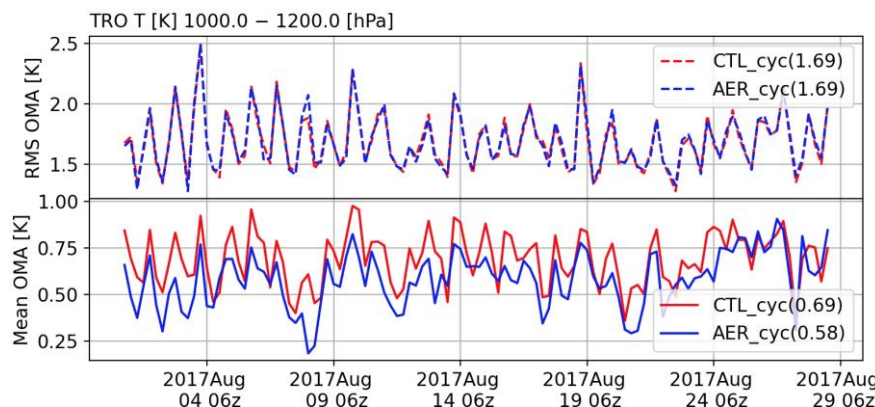
249

250

251

252

Figure 4 displays the statistics of analysis departures (observation minus analysis, OMA) from CTL_cyc and AER_cyc to evaluate the performance of temperature analysis at the lower atmosphere over the tropical region (20° S – 20° N). The positive value of mean OMAs indicates that both experiments have cold biases in the tropical region. It shows neutral impact on root-mean-square (RMS) and slightly positive impact on the cold biases. The latter implies that the departure of temperature analysis becomes larger when considering aerosol transmittance effects during the data assimilation (i.e., AER_cyc).



253
254 **Figure 4.** The comparison of the RMS and mean analysis departures (observation minus analysis, OMA) against in-situ
255 measurements (e.g., radiosonde) of temperature with pressure over 1,000 hPa at the tropical region (20° S – 20° N) during 00Z
256 August 1 – 18Z August 28, 2017.

257
258 Medium-range forecasts of AER_cyc are examined against CTL_cyc using the verification package from NOAA/NCEP EMC
259 (https://www.emc.ncep.noaa.gov/gmb/STATS_vsdb). Figure 5 displays the scorecard of anomaly correlation and root-mean-
260 square error (RMSE) for the day-1, -3, and -5 forecasts over August 1 – 28, 2017. Anomaly correlation coefficients show
261 neutral to positive impact on day-1 forecasts of wind and temperature fields when aerosol cooling effects in BTs are considered.
262 The RMSE scorecards show the improvement over the Northern Hemisphere (20° N – 80° N) and the Tropics (20° S – 20° N),
263 while neutral or degradation over the Southern Hemisphere (20° S – 80° S). Compared to both hemispheres, the tropical
264 forecasts show improved statistics in the aerosol-aware analysis, which may be attributed to larger aerosol loading in this
265 region. Overall, the aerosol-aware data assimilation provides neutral to slightly positive impacts on forecast skills. It should
266 be noted that evaluation of the aerosol impacts on the African easterly wave that developed Hurricane Harvey and Gert in 2017
267 has been presented in Grogan et al. (2021).

268



			Globe			N. Hemisphere			S. Hemisphere			Tropics				
			Day 1	Day 3	Day 5	Day 1	Day 3	Day 5	Day 1	Day 3	Day 5	Day 1	Day 3	Day 5		
Anomaly Correlation	Heights	250hPa														
		500hPa														
		700hPa														
		1000hPa														
	Vector Wind	250hPa	▲													
		500hPa	▲													
		850hPa	▲													
	Temp	250hPa														
		500hPa		▼												
850hPa		▲														
RMSE	Heights	10hPa	▲	▲	▲		▲	▲					▲	▲	▲	
		20hPa	▲	▲	▲	▲	▲	▲					▲	▲	▲	
		50hPa	▲	▲	▲	▲	▲	▲	▲				▲	▲	▲	
		100hPa	▲	▲	▲	▲	▲						▲	▲	▲	
		200hPa	▲											▲	▲	
		500hPa												▲	▲	
		700hPa														
		850hPa														
		1000hPa														
		Vector Wind	10hPa	▲	▲			▲	▲	▲					▲	▲
	20hPa		▲	▲			▲	▲	▲	▲				▲	▲	▲
	50hPa		▲	▲			▲	▲	▲	▲				▲	▲	▲
	100hPa		▲	▲	▲	▲	▲	▲	▲	▲				▲	▲	▲
	200hPa		▲				▲							▲	▲	
	500hPa		▲											▲	▲	
	700hPa		▲											▲	▲	
	850hPa		▲											▲	▲	
	1000hPa		▲											▲	▲	
	Temp		10hPa	▲	▲			▲							▲	▲
		20hPa	▲	▲			▲	▲	▲	▲				▲	▲	▲
		50hPa	▲	▲			▲	▲	▲	▲				▲	▲	▲
		100hPa	▲	▲			▲	▲	▲	▲				▲	▲	▲
		200hPa	▲				▲							▲	▲	▲
		500hPa														
		700hPa														
		850hPa														
		1000hPa														

269
 270 **Figure 5.** Scorecard of anomaly correlation and RMSE of comparison between AER_cyc and CTL_cyc. Green colors means
 271 AER_cyc is better than CTL_cyc at 95% (filled box), 99% (▲), and 99.9% (▲) significance level. Red colors means AER_cyc
 272 is worse than CTL_cyc at 95% (filled box), 99% (▼), and 99.9% (▼) significance level. Grey boxes mean no statistically
 273 significant difference between AER_cyc and CTL_cyc. Blue boxes are not statistically relevant. The statistics are calculated
 274 between 20 to 80 degrees of latitude for both hemispheres. The data between 20 °S and 20 °N is used for the tropical region.

275 **4. Conclusions and Future Outlook**

276 This article described aerosol absorption and scattering calculations of the CRTM version 2 in the GSI analysis. We also
 277 conducted sensitivity experiments to investigate the aerosol-affected GSI analysis in both single-cycle and fully-cycled runs.
 278 Both GSI and CRTM are well documented with user guides, tutorials and code repositories available online. This article is



279 primarily a joined-up documentation for aerosol absorption and scattering calculations in the CRTM version 2 and GSI. It also
280 provides guidance for prospective users of the CRTM aerosol option. Scientific aspects of aerosol-affected BT in atmospheric
281 data assimilation are briefly discussed. Specifically, numerical experiments were conducted to illustrate how including aerosol
282 radiative effects in CRTM changes the GSI analysis. We found that taking the aerosols into account reduces simulated BT in
283 thermal window channels over dust-dominant regions. Assimilating aerosol-affected BTs produces a warmer analyzed lower
284 atmosphere. From the verification scorecard, neutral to positive results are found in the fully-cycled, aerosol aware experiment.
285

286 The CRTM team, in coordination with its partners and collaborators, is building a robust capability to accurately and
287 consistently simulate the emission, absorption, and scattering properties of all (radiatively important) atmospheric constituents.
288 There are several ongoing and planned efforts to enhance the CRTM aerosol module. For example, more aerosol optical look-
289 up tables have been added and the calculations of aerosol optical properties are being evaluated. In addition, the CRTM is
290 being refactored toward a more flexible aerosol interface to handle aerosol optical look-up-tables as well as to support aerosol
291 specifications from other operational aerosol models, such as Community Multiscale Air Quality (CMAQ). Other aerosol-
292 related efforts include, but not limited to, improving the physical representation of aerosols and including active sensors such
293 as aerosol lidar. These developments, once implemented and tested, will be reported in future manuscripts.

294 **Code and Data Availability.**

295 Various software packages are referred to throughout the paper. The following list contain links to the main software
296 documentations or repositories discussed:

297 The GSI webpage: <https://dtcenter.ucar.edu/com-GSI/users/index.php>

298 The GSI v3.7 user guide: https://dtcenter.ucar.edu/com-GSI/users/docs/users_guide/html_v3.7/index.html

299 The GSI v3.7 online tutorial: https://dtcenter.ucar.edu/com-GSI/users/tutorial/online_tutorial/index_v3.7.php

300 The NOAA/NCEP/EMC GSI repository: <https://github.com/NOAA-EMC/GSI>

301 The CRTM webpage: <https://github.com/JCSDA/crtm/wiki>

302 The CRTM tutorial: <https://github.com/JCSDA/crtm/wiki/CRTM-Tutorial>

303 The CRTM repository: <https://github.com/JCSDA/crtm>

304 The CRTM User Guide: https://github.com/JCSDA/crtm/wiki/files/CRTM_User_Guide.pdf

305

306 The setup of CRTM functions for considering aerosol information can be found at Chapter 4 in the CRTM User Guide.

307 The aerosol related Fortran code in GSI (based on the structure of NOAA EMC GSI):

308 Aerosol files check (when `lread_ext_aerosol` is true): `./src/gsi/read_files.f90`

309 Aerosol data ingestion: `./src/gsi/ncep_nems_io.f90`, `./src/gsi/general_read_nems_aero.f90`



310 CRTM simulation: ./src/gsi/crtm_interface.f90
311 Effective radius setup: ./src/gsi/set_crtm_aerosolmod.f90

312 **Author Contributions.**

313 QL implemented the aerosol module, CL designed the experiments, and SW performed the experiments. CL prepared the
314 manuscript with contributions from all co-authors.

315 **Acknowledgements.**

316 The study of CTL and AER cycled experiments are supported by the Next Generation Global Prediction System (NGGPS)
317 program within NOAA/NWS (award number 352 NA15NWS4680008). The testing and refinement of GSI/CRTM regression
318 test is supported by the DTC Visitor Program. All experiments were conducted at NOAA/NESDIS-funded Supercomputer for
319 Satellite Simulations and Data Assimilation Studies (S4) cluster maintained by Space Science and Engineering Center (SSEC)
320 at University of Wisconsin-Madison. We thank GMAO collaborators, Arlindo da Silva, Mian Chin, and Peter Colarco, for
321 providing valuable input on the calculations of aerosol optical properties for GOCART aerosols.

322 **References**

- 323 d'Almeida, G. A., Koepke, P., and Shettle, E.P.: Atmospheric Aerosols: global climatology and radiative characteristics, A.
324 Deepak Publishing, Hampton, VA., 1991.
- 325 American Meteorological Society: Brightness Temperature. Glossary of Meteorology,
326 https://glossary.ametsoc.org/wiki/Brightness_temperature, 2012.
- 327 Binkowski, F. S., Roselle, S. J.: Models-3 Community multiscale air quality (CMAQ) model aerosol component, 1 Model
328 description. *J. Geophys. Res.*, 108, 4183, doi:10.1029/2001JD001409, 2003.
- 329 Buchard, V., da Silva, A. M., Colarco, P. R., Darmonov, A., Randles, C. A., Govindaraju, R., Torres, O., Campbell, J., and
330 Spurr, R.: Using the OMI aerosol index and absorption aerosol optical depth to evaluate the NASA MERRA Aerosol
331 Reanalysis. *Atmos. Chem. Phys.*, 15, 5743– 5760, doi:10.5194/acp-15-5743-2015, 2015.
- 332 Chin, M., Ginoux, P., Kinne, S., Torres, O., Holben, B. N., Duncan, B. N., Martin, R. V., Logan, J. A., and Higurashi, A.:
333 Tropospheric aerosol optical thickness from the GOCART model and comparisons with satellite and Sun photometer
334 measurements, *J. Atmos. Sci.*, 59, 461–483, doi:10.1175/1520-0469(2002)059<0461:TAOTFT>2.0.CO;2, 2002.



- 335 Chin, M., Diehl, T., Tan, Q., Prospero, J. M., Kahn, R. A., Remer, L. A., Yu, H., Sayer, A. M., Bian, H., Geogdzhayev, I. V.,
336 Holben, B. N., Howell, S. G., Huebert, B. J., Hsu, N. C., Kim, D., Kucsera, T. L., Levy, R. C., Mishchenko, M. I., Pan, X.,
337 Quinn, P. K., Schuster, G. L., Streets, D. G., Strode, S. A., Torres, O., and Zhao, X.-P.: Multi-decadal aerosol variations
338 from 1980 to 2009: a perspective from observations and a global model, *Atmos. Chem. Phys.*, 14, 3657–3690,
339 doi.org:10.5194/acp14-3657-2014, 2014.
- 340 Colarco, P., da Silva, A., Chin, M., and Diehl, T.: Online simulations of global aerosol distributions in the NASA GEOS-4
341 model and comparisons to satellite and ground-based aerosol optical depth, *J. Geophys. Res.*, 115, D14207,
342 doi:10.1029/2009JD012820, 2010.
- 343 Diaz, J. P., Arbelo, M., Expósito, F.J., Podesta', G., Prospero, J.M., and Evans, R.: Relationship between errors in AVHRR-
344 derived sea surface temperature and the TOMS Aerosol Index, *Geophys. Res. Lett.*, 28, 1989 – 1992, 2001.
- 345 Divakarla, M., and Coauthors: Evaluation of CrIMSS operational products using in-situ measurements, model analysis fields,
346 and retrieval products from heritage algorithms, IEEE International Geoscience and Remote Sensing Symposium, Munich,
347 Germany, 2012, pp. 1046-1049, doi: 10.1109/IGARSS.2012.6350818, 2012.
- 348 Gelaro, R., McCarty, W., Suarez, M. J., Todling, R., and coauthors, 2017: The Modern-Era Retrospective Analysis for
349 Research and Applications, Version 2 (MERRA-2). *J. Climate*, 30, 5419–5454, doi.org: 10.1175/JCLI-D-16-0758.1, 2017.
- 350 Grogan, D., Lu, C.-H., Wei, S.-W., and Chen, S.-P.: Effects of Saharan dust on African easterly waves: The impact of aerosol-
351 affected satellite radiances on data assimilation, *Atmos. Chem. Phys. Disc.*, doi:10.5194/acp-2021-129, 2021.
- 352 Hale, G. M. and Querry, M. R.: Optical constants of water in the 200-nm to 200-mm wavelength region. *Appl. Opt.*, 12, 555–
353 563, 1973.
- 354 Han, Y., van Delst, P., Liu, Q., Weng, F., Yan, B., Treadon, R., and Derber, J.: JCSDA Community Radiative Transfer Model
355 (CRTM) – Version 1, NOAA NESDIS Tech. Rep. 122, 33 pp., NOAA, Silver Spring, Md, 2006.
- 356 Han, Y., Weng, F., Liu, Q., and van Delst, P.: A fast radiative transfer model for SSMIS upper atmosphere sounding channels.
357 *J. Geophys. Res.*, 112, D11121, doi:10.1029/2006JD008208, 2007.
- 358 Hess, M., Koepke, P., Schult I: Optical properties of aerosols and clouds: the software package 1528 OPAC. *Bull Am Met Soc*
359 79:831–844, 1998.
- 360 Highwood, E. J., Haywood, J. M., Silverstone, M. D., Newman, S. M., and Taylor, J. P.: Radiative properties and direct effect
361 of Saharan dust measured by the C-130 aircraft during Saharan Dust Experiment (SHADE): 2. Terrestrial spectrum, *J.*
362 *Geophys. Res.*, 108(D18), 8578, doi:10.1029/2002JD002552, 2003
- 363 Kim, J., Akella, S., da Silva, A.M., Todling, R., McCarty, W.: Preliminary evaluation of influence of aerosols on the simulation
364 of brightness temperature in the NASA's Goddard Earth Observing System Atmospheric Data Assimilation System; Tech.
365 Rep. Ser. Glob. Model. Data Assim., Vol 49, TM–2018-104606, Goddard Space Flight Center, National Aeronautics and
366 Space Administration: Greenbelt, Maryland, US, 2018.
- 367 Kleist, D. T., Parrish, D. F., Derber, J. C., Treadon, R., Wu, W. S., and Lord, S.: Introduction of the GSI into the NCEP Global
368 Data Assimilation System. *Weather and Forecasting*, 24(6):16911705, 2009.



- 369 Letertre-Danczak, J.: The Use of Geostationary Radiance Observations at ECMWF and Aerosol Detection for Hyper-Spectral
370 Infrared Sounders: 1st and 2nd Years Report; EUMETSAT/ECMWF Fellowship Programme Research Reports, Vol 40,
371 European Centre for Medium Range Weather Forecasts: Shinfield Park, Reading, RG2 9AX, England, 2016.
- 372 Liu, Q. and Weng, F.: Advanced doubling-adding method for radiative transfer in planetary atmosphere, *J. Atmos. Sci.*, 63,
373 3459-3465, doi:10.1175/JAS3808.1, 2006.
- 374 Liu, Q., Han, Y., van Delst, P., and Weng, F.: Modeling aerosol radiance for NCEP data assimilation, in *Fourier Transform
375 Spectroscopy/Hyperspectral Imaging and Sounding of the Environment*, paper HThA5, OSA Technical Digest Series,
376 Optical Society of America, doi:10.1364/HISE.2007.HThA5, 2007.
- 377 Liu, Q. and Lu, C.-H.: Community Radiative Transfer Model for Air Quality Studies. In *Light Scattering Reviews*. 456
378 Kokhanovsky, A., Eds.; Springer Praxis Books, Springer-Verlag, Berlin – Heidelberg, Germany, Volume 457, pp. 67-115,
379 2016.
- 380 Liu, Z., Liu, Q., Lin, H.-C., Schwartz, C. S., Lee, Y.-H., and Wang, T.: Three-dimensional variational assimilation of MODIS
381 aerosol optical depth: Implementation and application to a dust storm over East Asia, *J. Geophys. Res.*, 116, D23206,
382 doi:10.1029/2011JD016159, 2011.
- 383 Lu, C.-H., da Silva, A., Wang, J., Moorthi, S., Chin, M., Colarco, P., Tang, Y., Bhattacharjee, P. S., Chen, S.-P., Chuang, H.-
384 Y., Juang, H.-M. H., McQueen, J., and Iredell, M.: The implementation of NEMS GFS Aerosol Component (NGAC)
385 version 1.0 for global dust forecasting at NOAA/NCEP, *Geosci. Model Dev.*, 9, 1905–1919, doi: 10.5194/gmd-9-1905-
386 2016, 2016.
- 387 Matricardi, M.: The inclusion of aerosols and clouds in RTIASI, the ECMWF fast radiative transfer model for the infrared
388 atmospheric sounding interferometer, *ECMWF Tech. Memo.*, 474, doi: 10.21957/1krvb28ql, 2005.
- 389 Merchant, C. J., Embury, O., Le Borgne, P. and Bellecm B.: Saharan dust in nighttime thermal imagery: Detection and
390 reduction of related biases in retrieved sea surface temperature, *Remote Sensing of Environ.*, 104, 15–30, doi:
391 10.1016/j.rse.2006.03.007, 2006.
- 392 Nalli, N. R., and L. L. Stowe, Aerosol correction for remotely sensed sea surface temperatures from the National Oceanic and
393 Atmospheric Administration advanced very high resolution radiometer, *J. Geophys. Res.*, 107(C10), 3172, doi:10.1029/
394 2001JC001162, 2002.
- 395 Pagowski, M., Liu, Z., Grell, G. A., Hu, M., Lin, H.-C., Schwartz, C. S., Implementation of aerosol assimilation in Gridpoint
396 Statistical Interpolation (v3.2) and WRF-Chem (v.3.4.1), *Geosci. Model Dev.*, 7, 1621–1627, doi:10.5194/gmd-7-1621-
397 2014, 2014.
- 398 Petty G: *A First Course in Atmospheric Radiation*, 2nd edition, Sundog Publishing, Madison, WI, 2006.
- 399 Peyridieu, S., Chdin, A., Tanr, D., Capelle, V., Pierangelo, C., Lamquin, N., and Armante, R.: Saharan dust infrared optical
400 depth and altitude retrieved from AIRS: a focus over North Atlantic comparison to MODIS and CALIPSO, *Atmos. Chem.
401 and Phys. Discuss.*, 9(5):2119921235, 2009.



- 402 Pierangelo, C., Chedin, A., Heilliette, S., Jacquinet-Husson, N., and R. Armante, R.: Dust altitude and infrared optical depth
403 from AIRS. *Atmos. Chem. Phys.*, 4, 1813-1822, doi: 10.5194/acp-4-1813-2004, 2004.
- 404 Randles, C. A., da Silva, A. M., Buchard, V., Colarco, P. R., Darmenov, A., Govindaraju, R., Smirnov, A., Holben, B., Ferrare,
405 R., Hair, J., Shinozuka, Y., Flynn, C., J: The MERRA-2 Aerosol Reanalysis, 1980 Onward. Part I: System Description and
406 Data Assimilation Evaluation, *Journal of Climate*, 30(17), 6823-6850, doi:10.1175/JCLI-D-16-0609.1, 2017.
- 407 Schwartz, C. S., Liu, Z., Lin, H.-C., and Cetola, J. D.: Assimilating aerosol observations with a “hybrid” variational-ensemble
408 data assimilation system, *J. Geophys. Res.-Atmos.*, 119, 4043–4069, doi:10.1002/2013JD020937, 2014.
- 409 Sokolik, I. N.: The spectral radiative signature of wind-blown mineral dust: Implications for remote sensing in the thermal IR
410 region: The spectral radiative signature of wind-blown mineral dust, *Geophys. Res. Lett.*, 29, 7-1-7-4,
411 doi:10.1029/2002GL015910, 2002.
- 412 Stegmann, P. G., Tang, G., Yang, P. and Johnson, B. T.: A stochastic model for density-dependent microwave Snow- and
413 Graupel scattering coefficients of the NOAA JCSDA community radiative transfer model, *J. Quant. Spec. Rad. Trans.*,
414 211, 9-24, doi:10.1016/j.jqsrt.2018.02.026, 2018.
- 415 Ukhov, A., Ahmadov, R., Grell, G., and Stenchikov, G.: Improving dust simulations in WRF-Chem model v4.1.3 coupled
416 with GOCART aerosol module, *Geosci. Model Dev. Disc.*, doi:10.5194/gmd-2020-92, 2021.
- 417 Wang, J., Bhattacharjee, P.S., Tallapragada, V., Lu, C.-H., Kondragunta, S., da Silva, A., Zhang, X., Chen, S.-P., Wei, S.-W.,
418 Darmenov, A.S., et al.: The implementation of NEMS GFS Aerosol Component (NGAC) Version 2.0 for global
419 multispecies forecasting at NOAA/NCEP – Part 1: Model descriptions., *Geosci. Model Dev.*, 11, 2315–2332,
420 doi:10.5194/gmd-11-2315-2018, 2018.
- 421 Weaver, C. J., Joiner, J., and Ginoux, P.: Mineral aerosol contamination of TIROS Operational Vertical Sounder (TOVS)
422 temperature and moisture retrievals., *J. Geophys. Res.*, 108, doi:10.1029/2002JD002571, 2003.
- 423 Wei, S.-W., Lu, C.-H., Liu, Q., Collard, A., Zhu, T., Grogan, D., Li, X., Wang, J., Grimble, R., and Bhattacharjee, P.: The
424 impact of aerosols on satellite radiance data assimilation using NCEP global data assimilation system, *Atmos.*, 12(4), 432,
425 doi:10.3390/atmos12040432, 2021.
- 426 Weng, F.: Advances in radiative transfer modeling in support of satellite data assimilation. *J. Atmos. Sci.*, 64, 3799–3807,
427 doi:10.1175/2007JAS2112.1, 2007.
- 428 Wu, W.-S., Purser, R. J., and Parrish, D. F.: Three-dimensional variational analysis with spatially inhomogeneous covariances,
429 *Mon. Weather Rev.*, 130, 2905–2916, doi:10.1175/1520-0493(2002)130<2905:TDVAWS>E2.0.CO;2, 2002.
- 430 Zhang L., Grell, G.A., Montuoro, R., McKeen, S. A., Bhattacharjee, P. S., Baker, B., Henderson, J., Pan, L., Frost, G. J.,
431 McQueen, J., Saylor, R., Ahmadov, R., Li, H., Wang, J., Stajner, I., Kondragunta, S., Zhang, X., Li, F.: Development of
432 GEFS-Aerosols into NOAA's Unified Forecast System UFS., In preparation, 2021.